
Article:
Rajana, K, Tsavdaridis, KD orcid.org/0000-0001-8349-3979 and Koltsakis, E (2020) Elastic and inelastic buckling of steel cellular beams under strong-axis bending. Thin-Walled Structures, 156. 106955. ISSN 0263-8231

https://doi.org/10.1016/j.tws.2020.106955

Elastic and Inelastic Buckling of Steel Cellular Beams under Strong-Axis Bending

Komal Rajana[1], Konstantinos Daniel Tsavdaridis[2*] and Efthymios Koltsakis[3]

[1]PhD Student, School of Mathematics, Computer Science and Engineering, Civil Engineering, City, University of London, EC1V 0HB, London, UK

[2]Associate Professor of Structural Engineering, School of Civil Engineering, Faculty of Engineering and Physical Sciences, University of Leeds, LS2 9JT, Leeds, UK

[3]Associate Professor, Department of Civil Engineering, Aristotle University of Thessaloniki, Greece

[*]*Corresponding author,* E-mail: K.Tsavdaridis@leeds.ac.uk

ABSTRACT

This paper presents an extensive parametric study of elastic and inelastic buckling of cellular beams subjected to strong axis bending in order to investigate the effect of a variety of geometric parameters, and further generate mass data to validate and train a neural network-based formula. Python was employed to automate mass finite element (FE) analyses and reliably examine the influence of the parameters. Overall, 102,060 FE analyses were performed. The effects of the initial geometric imperfection, material nonlinearity, manufacture-introduced residual stresses, web opening diameter, web-post width, web height, flange width, web and flange thickness, end web-post width, and span of the beams and their combinations were thoroughly examined. The results are also compared with the current state-of-the-art design guidelines used in the UK.

It was concluded that the critical elastic buckling load of perforated beams corresponds to the lateral movement of the compression flange while the most critical parameters are the web thickness and the geometry of the flange. However, from the inelastic analysis, the geometry and position of the web opening influence the collapse load capacity in a similar fashion to the geometry of the flange and thickness of the web. It was also concluded that the effect of the initial conditions was insignificant.

Keywords: Cellular beams; Elastic and inelastic buckling; Strong-axis bending; FEA; Parametric studies; Automated analyses; Python; Mass data

1. Introduction

1.1 Background

The use of steel beams is an attractive option within the steel construction industry due to its flexibility in terms of strength, size, and weight. The most notable benefits of perforated beams are the inclusion of services, thereby reducing the building's height, the need for internal columns, construction time and costs. The increased depth of cellular beams offers greater bending resistance in the strong-axis which provides an increased moment of inertia when compared to similar weight sections.

Perforated beams with circular web openings referred to as cellular beams have been found to have additional merits relating to its flexibility and design when compared to other beams with varying opening shapes. The presence of web openings, however, presents several intricate behavioural patterns due to the combined shear and bending stresses concentrated at the openings. According to Ward (1990) the load-carrying capacity of a cellular beam is significantly affected by the response of the web-post and the tee-sections to local bending and vertical shear across the web opening. Consequently, over the years, researchers have studied the stress distribution pattern and failure modes of these beams based on elastic and inelastic behavioural patterns. Figure 1 displays a cellular perforated section in static equilibrium.

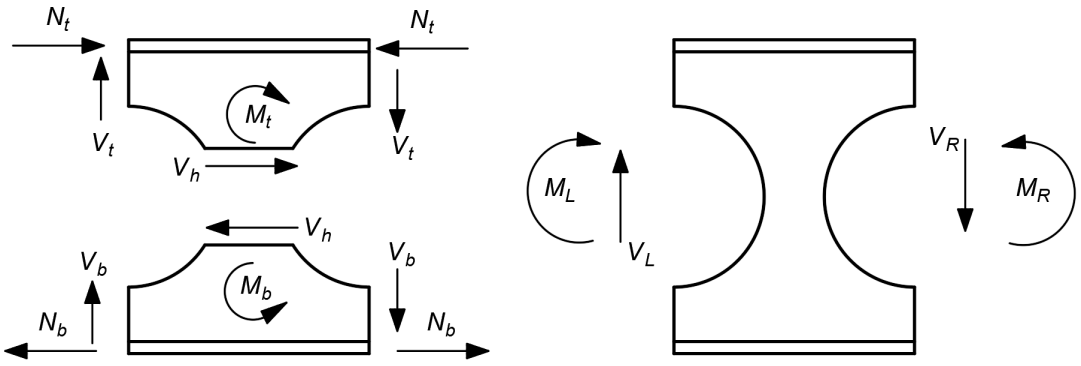

Figure 1: Forces in static equilibrium at the opening and the web-post

The aim of the current study is to highlight the effects of certain key parameters (e.g., material nonlinearities, manufacture-introduced residual stresses, web opening diameters, web-post widths, heights of web, widths of flange, flange thicknesses, web thicknesses, and lengths of beams) on the global structural behaviour and ultimate load capacity through developing mass data. The global response was considered as a combined interaction of the global lateral buckling mode and localised deformations at the openings. The interaction of buckling modes in I-section beams (perforated and non-perforated) has been a subject of extensive experimental and numerical investigations. For example, Bradford (1992, 1998) thoroughly examined the lateral-distortional buckling of I-sections, Zirakian and Showtaki (2006) was one of the first to study the distortional buckling of castellated beams, also Zirakian (2008) studied the elastic distortional buckling of doubly symmetric I-shaped flexural members with slender webs, and Ellobody (2011, 2012, 2017) comprehensively investigated the interaction of buckling modes in castellated steel beams conducting nonlinear analyses under combined buckling modes as well as studying the interaction of buckling modes in steel plate girders. Ellobody (2012) concluded that the influence of the interactions of lateral-torsional and web distortional buckling of cellular beams on the strength and inelastic behaviour is yet to be

understood. As such, this research sought to avoid the analysis of many complex localised failures associated with cellular beams by utilising a FE collapse analysis to compute the global buckling capacity as a Load Proportionality Factor (LPF) of the entire beam. Even though many researchers since 1957 (e.g., Altfillisch et al., 1957, Kolosowski J, 1964, etc.) investigated perforated beams; until the past decade where scientists have studied various locatlised failures such as buckling (e.g., Ellobody, 2011) and vertical shear, aka Vierendeel (e.g., Tsavdaridis and D'Mello, 2012; Tsavdaridis and Galiatsatos, 2015), very little has been done with regards to the global response of such members.

With the power of todays' FE tools and CPU, this study provides an opportunity to fill this gap in the literature, as extensive FE parametric analyses on the structural stability of thin-walled cellular beams can attempt to clarify the influence of each parameter to the perforated beams' complex structural behaviours.

1.2 Failure Modes

Past numerical and experimental studies on perforated beams have shown that the failure modes are dependent on the slenderness of the section, the geometry of the web opening (i.e., diameter and web-post) and the type of load application (Chung et al., 2003). The bending and shear stresses concentrate in the vicinity of the openings and trigger several types of failure modes including web-post buckling, lateral-torsional buckling (LTB) with web-distortion, Vierendeel mechanism and the rupture of the welded joints.

The excessive plastification of plastic hinges, or Vierendeel mechanism, commonly occurs in beams with short spans, wide web-post, width flange, and shallow tee-sections. This type of failure was firstly reported by Alfifillisch et al. in 1957 and later by Kolosowski, 1964, while it was comprehensively studied by Kerdal and Nethercot (1984) to develop an in-depth understanding of the effects of the opening geometry. The past decade, Tsavdaridis et al. presented a series of extensive research studies investigating the mobility and position of plastic hinges when different shape and size of web openings are used and relate them with the shear-moment interaction at the centreline of the particular opening. Experimental (Tsavdaridis 2010; Tsavdaridis and D'Mello 2012) and FE (Tsavdaridis and D'Mello, 2009; Tsavdaridis and D'Mello, 2011) studies have been conducted. Moreover, Kingman et al. (2015) proposed optimised architectures for web openings to better control the position of the plastic hinges, increasing the capacity of the section. Tsavdaridis and Galiatsatos (2015) have also studied the position of the plastic hinges and capacity gains by the introduction web-welded stiffeners. Yu et al. (2010) and Tsavdaridis et al. (2013) also studied the vertical shear capacity of such perforated sections when infilled by concrete. Later, Maraveas et al. (2017) has examined the performance of such beams under fire conditions too. Overall, it was concluded that the position of the plastic hinges drastically influences the beam's load-carrying capacity.

This study seeks to activate a lateral global buckling failure combined with a localised web-post deformation by alternating various magnitude of geometrical imperfections to the first global and local buckling modes. Therefore, the collapse failure (e.g., at maximum LPF) is in the form of a lateral distortional buckling (LDB) which consists of a combined effect of lateral movement, unequal twisting of the flange and localised web distortion of the cross-section.

1.3 Design Guidelines

Akrami and Erfani (2016) compared the most prevalent design guidelines and concluded that the methods proposed by Chung et al. (2003) and Tsavdaridis and D'Mello (2012) were the least restrictive as compared to the other design methods (i.e., ASCE 23-97; SCI-P100; SCI-P355) and produced the lowest errors. However, even though design methods have been presented, there are still several uncertainties that result in conservative and complicated design approaches. Therefore, the complexity of perforated beams and the numerous parameters which affect the performance indicate the need for further research - most importantly in the global response. In the design guidelines, some of the failure modes or a combination of failure modes and parameters are excluded, thus they are restrictive approaches.

2. Parametric Matrix and Finite Element Modelling

The variables required for the elastic analysis is only based on the linear elastic stiffness, boundary conditions, and geometry. The parametric study required the creation of 405 ABAQUS CAE base models. The non-scripted parameters were the spacing of web opening (3 values), the diameter of web opening (3 values), the height of section (3 values), the width of the flange (3 values) and length of member (5 values).

The total number of combinations generated with Python for each analysis type is as follow:

- Elastic analysis = 3^6 (x 5 lengths) = 3,645 FE simulations
- Nonlinear analysis = 3^9 (x 5 lengths) = 98,415 FE simulations

The critical geometrical parameters are provided in Figure 2.

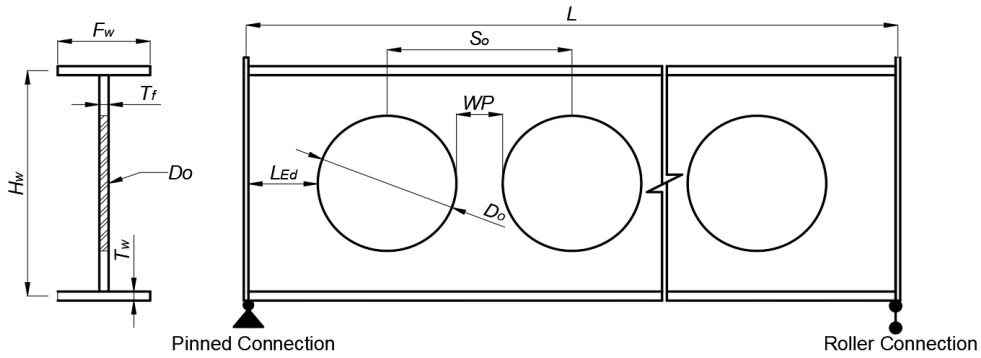

Figure 2: Important dimensional parameters of cellular beams

2.1 Geometric Parameters of Cross-Section

The lengths of beams selected for this study were 4m, 5m, 6m, 7m, and 8m. It was decided not to examine longer beams as the effect of the web opening is less critical to local failure mechanisms. According to Chung et al. (2001) and Tsavdaridis (2010) the longer the beam is, the less is the effect of the web opening position – a critical parameter for this study. When perforated sections with large web openings are considered, the combination of the beam span and the web opening position could yield completely different results. In particular, for long span beams (>7m) and web openings located close to the mid-span; the global bending moment at the perforated section increases quickly while the shear force decreases steadily. Therefore, the beams tend to fail in flexure due to a reduced moment capacity of the perforated

section. However, for short span beams a reduced load carrying capacity is obtained when the web openings are located either close to the supports or close to the mid-span. Obviously, the reduction of the shear capacity for large web openings close to the support is more severe. For conservative reasons, it is decided to use spans up to 8m for this research programme as the fluctuation of the results using large web openings leads to important conclusions. The fillet radius has been neglected in high impact research relating to cellular beams (Ellobody E, 2012; Tsavdaridis and D'Mello, 2011, 2012; Wang, Ma and Wang, 2014) and design guidelines (AISC, 2017), therefore, the influence is considered insignificant to alter the beam's global response, and it is not considered as a parameter variable for this study. This assumption is also in line with Sonck (2014) and Taras (2010) who have reported that this simplification by ignoring the fillet radius effects is small on the buckling curve parameters. This approach is also conservative and covers the case where fabricated sections are considered. The cross-section properties of the beams are summarised in Table 1.

Table 1: Cross-sectional description of beams

Description	Variable (1) (mm)	Variable (2) (mm)	Variable (3) (mm)
Web height (H_w)	700	560	420
Web thickness (T_w)	15	12	9
Flange width (F_w)	270	216	162
Flange thickness (T_f)	25	20	15

2.2 Web Opening Limits

The web opening diameter and spacing were limited to the recommended range in accordance with SCI-P100 (H_w/D_o=1.25 to 1.7 and S_o/D_o= 1.1 to 1.49). Table 2 provides the geometrical parameters for the perforation. It is worth noting that the location of the first web opening in the parametric study was placed at the centre of the beam while the subsequent adjacent openings were offset from the central opening until no more web opening can fit in the beam's length. This approach resulted in 135 different distances from the end perforation to the support (centreline of end-plate) which was also considered as an independent variable (L_{Ed}).

Table 2: Spacing between web openings with respect to the opening diameter

(H_w) (mm)	Do (mm) $(H_w/1.25, H_w/1.5$ & $H_w/1.7)$	(So) (mm)			WP (mm)		
		$1.1D_O$	$1.29D_O$	$1.49D_O$	$D_O/10$	$D_O/3.45$	$D_O/2.04$
700	560	616	722	834	56	162	274
	467	514	602	696	48	135	229
	412	453	531	613	41	119	202
560	448	493	578	668	45	130	220
	373	410	481	556	37	108	183
	329	362	424	490	33	95	161
420	336	370	433	501	37	97	165
	280	308	361	417	28	81	137
	247	272	319	368	25	72	121

2.3 Material Properties

The material behaviours used are elastic and elasto-plastic with isotropic strain hardening, which considered a tangential modulus of (E_t) 1000MPa, a Modulus of Elasticity of (E) 200GPa, and a Poisson's ratio of 0.3. The Tangent modulus assumption utilised after a detailed study of the test data taken from Redwood and McCutcheon (1968). The three combinations selected are presented in Table 3.

Table 3: Material nonlinearities for the three selected strength class for steel

Yield stress (MPa) f_y	**Ultimate stress (MPa)** f_u	**Initial Strain** (ε_y) f_y/E	**Final Strain** (ε_t) $\varepsilon_y + (f_u - f_y)/E_t$
235	360	0.001175	0.156775
355	510	0.001775	0.126175
440	550	0.0022	0.1122

2.4 Finite Element Properties

The geometry of the models was prepared using planar shell models having homogenous material properties. The finite element mesh uses the quad-dominated, type S8R (e.g., stress-displacement shell with eight nodes) doubly curved thick shell elements using reduced integration element which has six degrees of freedom per node. Sonck (2014) reported this is ideal for modelling cellular beams as hour-glassing would occur for the reduced order shell elements (e.g., S4R and S4R5). The consideration for the mesh was taken from Hesham Martini (2011) and Sweedan, (2011) where 12 elements are across the flange width and size for the web region was reduced by 20% (e.g., $F_W/12*1.2$). Support endplate uses 8 elements as this is unimportant. This arrangement has been observed, to accurately predict the global response of cellular beams tested in laboratory by Surtees and Liu (1995) and Tsavdaridis and D'Mello (2011) as detailed in section 3.0 and was effectively implemented for computational application in Abambres et al. (2018).

2.5 Boundary and Loading Conditions

The models considered a simple supported connection where one end was pinned and the other was a roller. This allowed an in-plane rotation but not a translation at one end while the other one permits the translation of the beam beyond the in-plane rotation point. Twisting rotations at the ends were prevented by restraining both the top and bottom flange tips against out-of-plane displacements. (Ellobody, 2012) A uniformly distributed unit load was applied to the top flange which gives the critical buckling load and the collapse load LPF as a multiplier of 1.0.

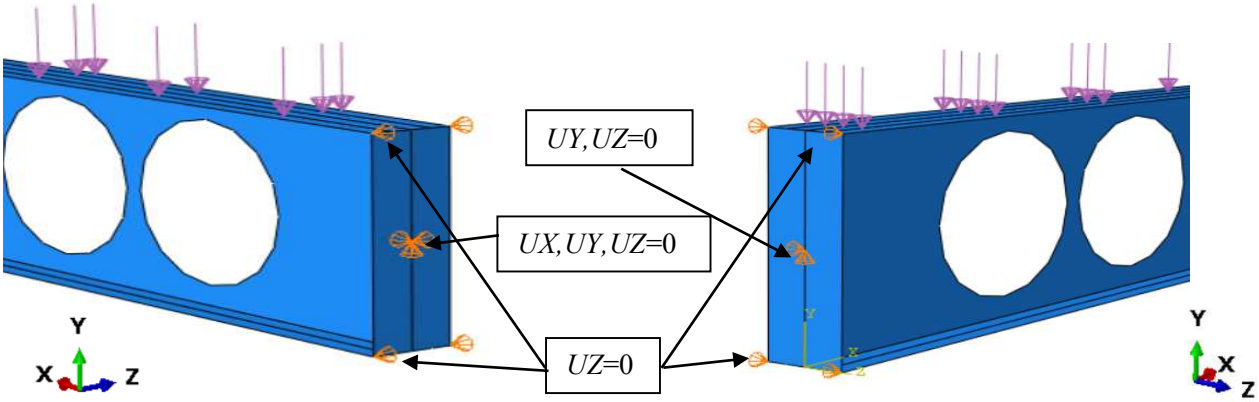

Figure 3: Boundary conditions in the finite element model

2.6 Initial Geometric Imperfection

Imperfections allow the initiation of buckling failure; however, this imperfection must be of small magnitude in order to avoid disruption of the beam's main responses. The global imperfection was applied to the first Eigen buckling mode and the local imperfection to the second or third Eigen buckling mode. As the beam length increases, the first two modes produced global perturbation shapes. The global imperfections (δ_g) scale was taken as $L/2500$, $L/2000$, and $L/1500$.

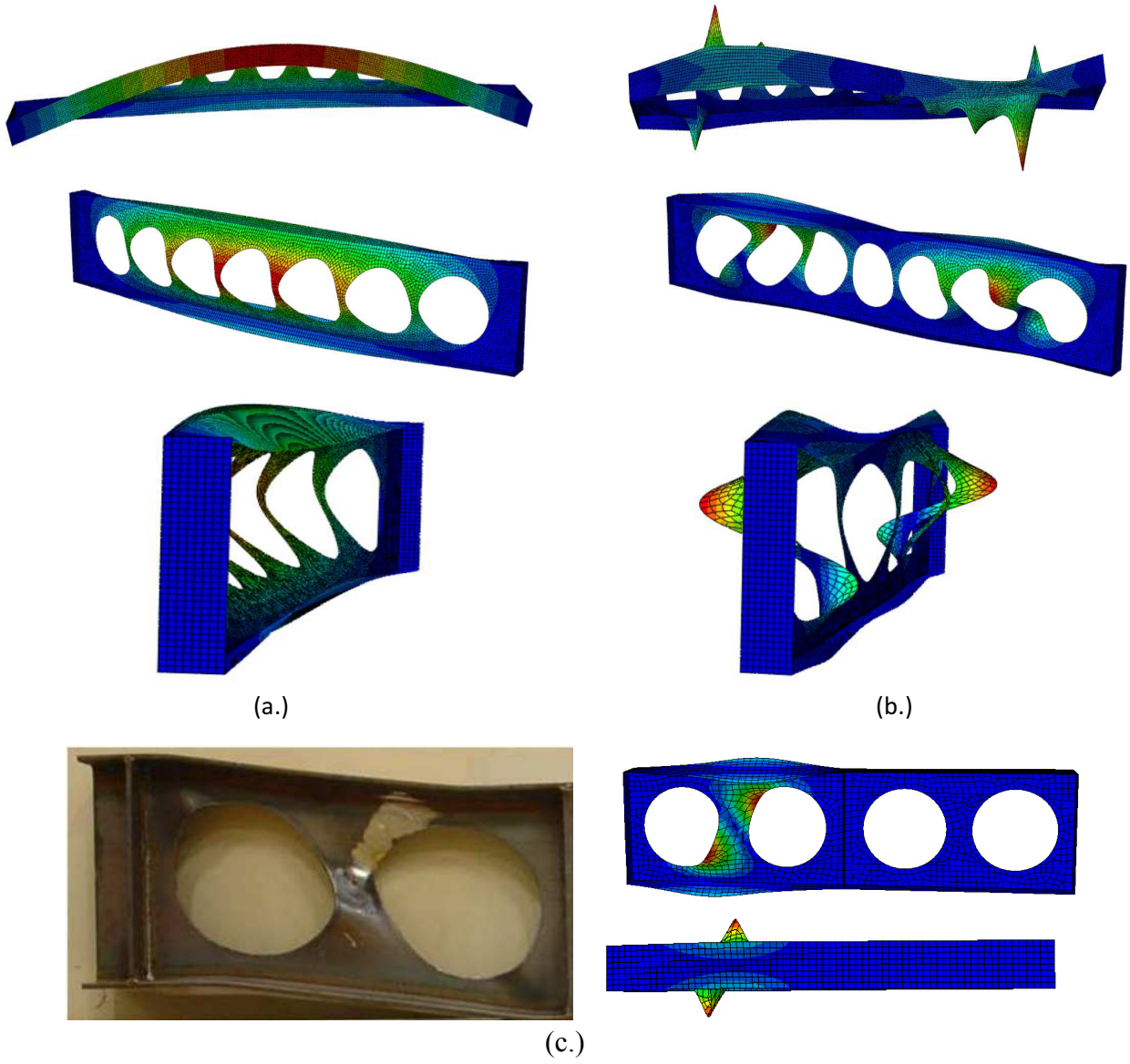

Figure 4: Perturbed geometry: (a) the global, (b) local initial geometrical imperfection shapes (local buckling near the supports), (c) Image of local imperfection (Tsavdaridis and D'Mello, 2011)

The local imperfection was based on Dawson and Walker (1972) method which is a function of the cross-section of the beam and the yield strength of steel. The following equations were utilised to calculate the

local imperfection for the web region as provided in Table 4. This imperfection shape only captured the web distortion buckling mode. The calculations incorporated a yield strength (f_y) of 355MPa.

$$\delta_{LI} = \frac{\gamma T_w f_y}{\sigma_{cr.l}} = \frac{\gamma f_y (H_w)^2}{21.6E.T_w} \quad \text{(eq1)}$$

$$\sigma_{cr.l} = \frac{23.9\pi^2 E}{12(1\text{-}0.3^2)}\left(\frac{T_w}{H_w}\right)^2 = 21.6E\left(\frac{T_w}{H_w}\right)^2 \quad \text{(eq2)}$$

The third local geometrical imperfection was chosen based on the following parameters in order to considered a localised imperfection that is slightly higher than what is specified by Dawson and Walker (1972).

$$\delta_{\mathrm{LI}(3)} = \frac{\left(\frac{\mathrm{F_W}}{2}\right)}{200} = \frac{c_{flange}}{200} \quad \text{(eq3)}$$

Table 4: Local web imperfection applied to the web buckling deformed mode

Formulae	T_w = 15mm H_w = 700mm	T_w = 12mm H_w = 560mm	T_w = 9mm H_w = 420mm
$\delta_{LI(1)} = \frac{0.1T_w f_y}{\sigma_{cr.l}}$	0.268441358	0.214753086	0.161064815
$\delta_{LI(2)} = \frac{0.2T_w f_y}{\sigma_{cr.l}}$	0.536882716	0.429506173	0.32212963
$\delta_{LI(3)} = \frac{c_{flange}}{200}$	0.675	0.54	0.405

2.7 Residual Stresses

During the cutting and welding process, the use of heat can lead to uneven cooling along with the member resulting in variable yield stress patterns and further differential plastic deformations (Sonck, 2014). The process of welding can cause a thermal contraction as the beam cools which may result in residual tension in the areas of the weld; as this takes longer to cool and compression in sections further away from the welded region may occur (Sonck, 2014; Sehwail, 2013). The residual stress pattern shown in Figure 5 was based on the findings reported by Snock (2014) for cellular beams where the web of the beam is subjected to tensile stresses. The flange has both tension and compression stresses similar to those presented by Tebedge (1973).

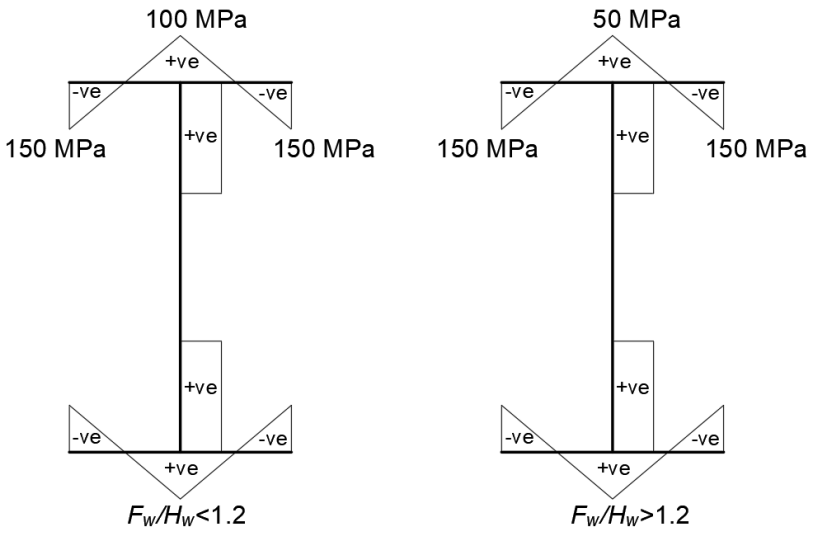

Figure 5: Residual stress pattern employed

2.8 Inelastic Analysis (Static Riks Method)

The static Riks method has the ability to keep the beam in equilibrium at every load increment during unstable phases of the analysis. Therefore, the analyses do not terminate at maximum LPF and then go into a snap-through response as the beam's geometry changes which yields a lower LPF in the parametric study. Due to no stopping criterion at maximum LPF in ABAQUS, the arc-length increment was specified for each of the 405 models in the Python script to allow for the termination of the analyses before the onset of the snap-through response. This was done by monitoring 405*3 = (1215) simulations.

2.9 Application of Geometric Imperfections and Residual Stresses

The initial geometric imperforation was introduced by using the perturbation in the geometry generated from the elastic buckling analysis by applying a scale factor (local and global imperfection). Following the introduction of the initial stresses, a general static step was required to allow the beam to regain its equilibrium before the load step. The static Riks step was then introduced to continue the analysis into the nonlinear response.

2.10 LPF Output

To establish LPF as a variable, it was required to request all displacement history output for a particular node in the model. The location of the node selected in the model is insignificant as LPF output variable is for the entire model response, therefore, in the Python script, a 'gather' and 'output' command was used to extract the LPF for a specific increment at maximum LPF.

3. FE Validation Study

The FE models were validated employing two experimental models found in the literature (Tsavdaridis and D'Mello, 2011; Surtees and Liu, 1995), including the response of a short beam to local web-post buckling failure and a longer beam to capture the global response with the combination of web distortional buckling.

Both validations were considered satisfactory with results within 3% of the load capacity recorded by the experiment. In Figure 5.a, the collapse load (P_{CL}) computed was 0.52 * 572,009N (e.g., Eigen-mode 1, elastic buckle load 572,009N) = 297kN and the experimental results is 288.7kN in Tsavdaridis and D'Mello (2011) for a 1.7m length beam. For a longer restrained/braced beam, the experiment P_{CL} by Surtees and Liu (1995) is 188.5kN and in Figure 5.b the LPF is 1.87 (e.g., 1.87*100,000N is 187kN). Therefore, it is safe to conclude that the Methodology adopted provides accurate results. For more information, please refer to Tsavdaridis and D'Mello (2011).

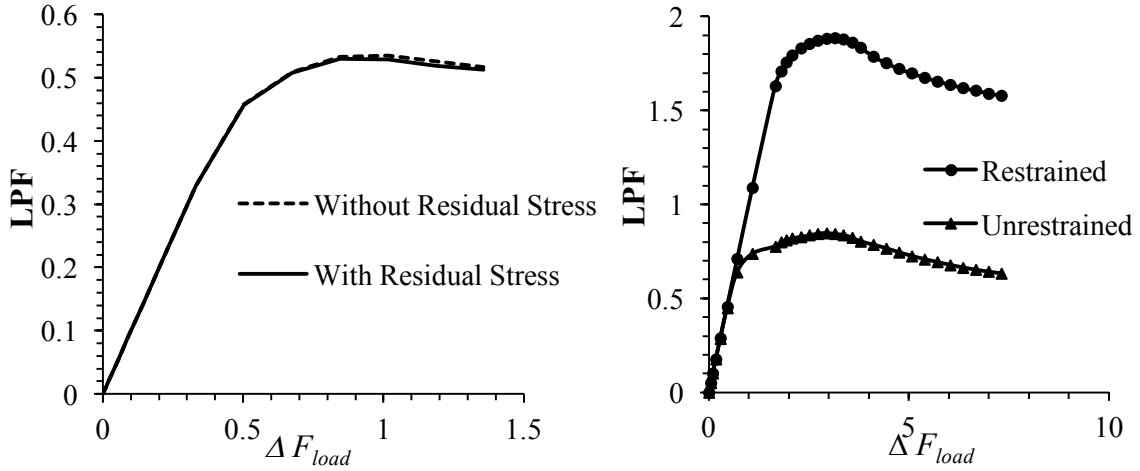

Figure 6: Collapse loading (LPF) of the beam. (a) Tsavdaridis and D'Mello, 2011 and (b) Surtees and Liu, 1995

4. Results and Discussion

4.1 FEA and SCI P355 Results

Figure 7 demonstrates that the SCI P355 analytical method produced conservative load-carrying capacities as compared to that of the FEA models. It is also noticeable that the differences between the two computational methods do not produce a similar percentage of variance (pattern) in the load-carrying capacity for the 8 selected beams, while the inelastic results are compared very well with the SCI P355 calculation. For example, beam 'A11' and beam 'A25' has a percentage variance of 6% and 45%, respectively. Beam 'A11' shows that the SCI P355 overestimated the capacity because the end distance from the last opening to the edge of the beam was not incorporated in the SCI design calculations. On the contrary, the narrow end distance which governed the analysis in FEA. In another case, beam 'A25', where the end distance is larger, SCI P355 method resulted in a very conservative low load as compared to the FEA, while the web-post buckling would always govern the design using the SCI P355 for beams with slender web-posts (i.e., closely spaced web openings). Therefore, for slender WP, web buckling will always govern the design in SCI P355. As for the FEAs, the end distance parameter governs the design for widely spaced web openings. It is worth to note that SCI P355 does not consider L_{Ed} but recommends $\geq 0.5D_o$.

It should be noted, that the simple strut approach model adopted in SCI P355 underestimates the true capacity of the web-post for slender wed-post (e.g., $D_o/3.45$ to $D_o/10$) and a revision is necessary to improve the accuracy. However, SCI P355 provides accurate results for widely spaced openings (e.g., web-post > $D_o/3.45$) as the Vierendeel bending approach adopted is suitable to estimate the shear across the opening.

Table 5 - Independent variable combination for SCI P355 design comparison

Ref #	L(mm)	T_w (mm)	T_f (mm)	F_w (mm)	H_w (mm)	D_o (mm)	WP (mm)
A10	4000	9	15	162	560	448	45 *
A11					560	448	130 **
A16					560	329	33 *
A17					560	329	95 **
A19					420	336	34 *
A20					420	336	97 **
A25					420	247	25 *
A26					420	247	72**

* = $0.1d_o$
** = $0.3\ d_o$

Figure 7 includes the elastic buckling load (Υ_{cr}) is considerably high which concludes that the Υ_{cr} should be used with caution as imperfection and initial stresses are always present. The Υ_{cr} seems to be in the region of approximately 45% more than the nonlinear buckling load.

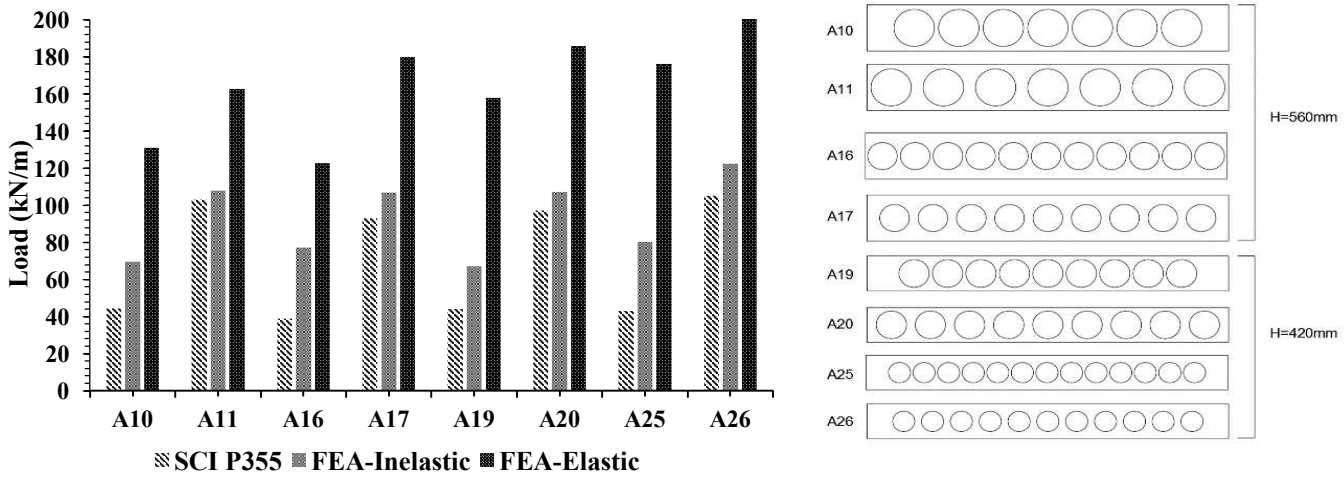

Figure 7: SCI P355, inelastic and elastic buckling load comparison, L = 4m

4.2 Results of Elastic Analyses

This section contains an analysis of the relationships of the effects of the independent variables on the dependent out variable (Υ_{cr}). The graphs were analysed with respect to the T_w and D_o as a function of the H_w. Figure 8 demonstrates the effects of the length (L) and H_w with the constant parameters Do/WP = 10, F_w = 162mm and T_f = 15mm.

In Figure 8, the H_w is an insignificant parameter since the first buckling mode corresponded to a lateral buckling and therefore the F_w is a critical parameter to restraint the lateral movement. The effects of D_o (e.g., H_w/D_o = 1.25 to 1.7) and the effects of T_w (e.g., 9mm to 15mm) are as follow:

- $5.5 \geq L/H_w \leq 7.5$, D_o effects are approximately 10.5% and T_w increases the Υ_{cr} by about 98%.
- $7.5 \geq L/H_w \leq 10.5$, D_o effects are approximately 7.5% and T_w increases the Υ_{cr} by about 62%.
- $10.5 \geq L/H_w \leq 13.5$, D_o effects are approximately 7.0% and T_w increases the Υ_{cr} by about 45%.
- $13.5 \geq L/H_w \leq 19$, D_o effects are approximately 6.5% and T_w increases the Υ_{cr} by about 30%.

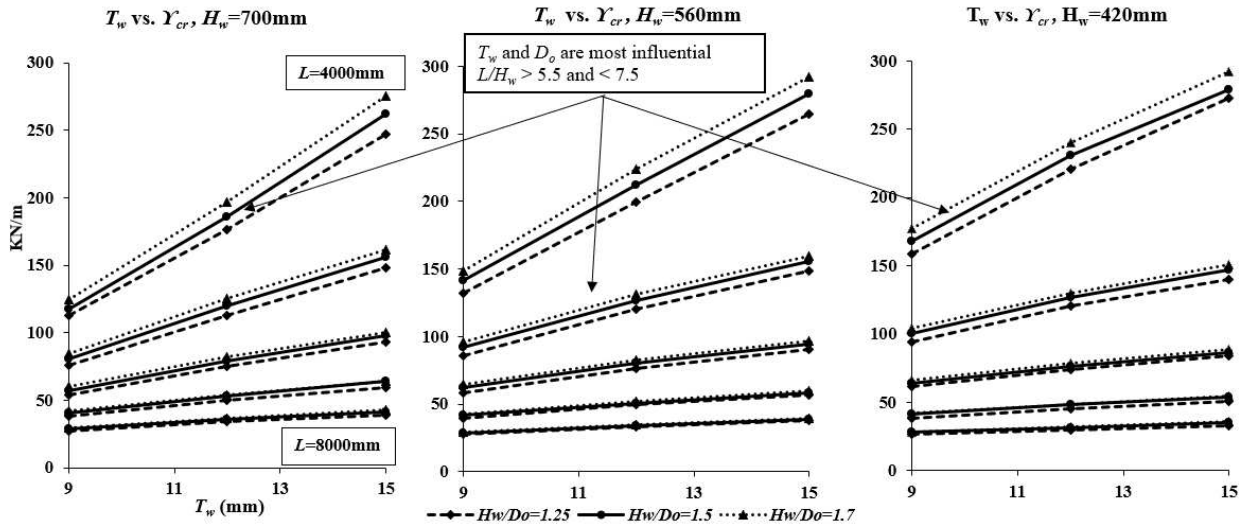

Figure 8: Effects of H_w on the elastic load (Υ_{cr}) with respect to varying T_w and L: 4m to 8m

In Figure 9, the F_w was increased from 162mm to 270mm. The change in F_w positively impacted the Υ_{cr} as lateral movement is restricted and the gradient of the plot increased greatly with the change in T_w (e.g., 15mm to 25mm). The following was concluded:

- $5.5 \geq L/H_w \leq 7.5$, D_o effects are approximately 14% and T_w increases the Υ_{cr} by about 150%.
- $7.5 \geq L/H_w \leq 10.5$, D_o effects are approximately 11.5% and T_w increases the Υ_{cr} by about 140%.
- $10.5 \geq L/H_w \leq 13.5$, D_o effects are approximately 8.5% and T_w increases the Υ_{cr} by about 110%.
- $13.5 \geq L/H_w \leq 19$, D_o effects are approximately 5.5% and T_w increases the Υ_{cr} by about 45%.

Comparing Figures 8 and 9 by increasing the F_w for critical members (e.g., $5.5 \geq L/H_w \leq 7.5$) the load increased is in the region of 85% and for slightly less slender members (e.g., $7.5 \geq L/H_w \leq 10.5$) the F_w effects has increases to 135%.

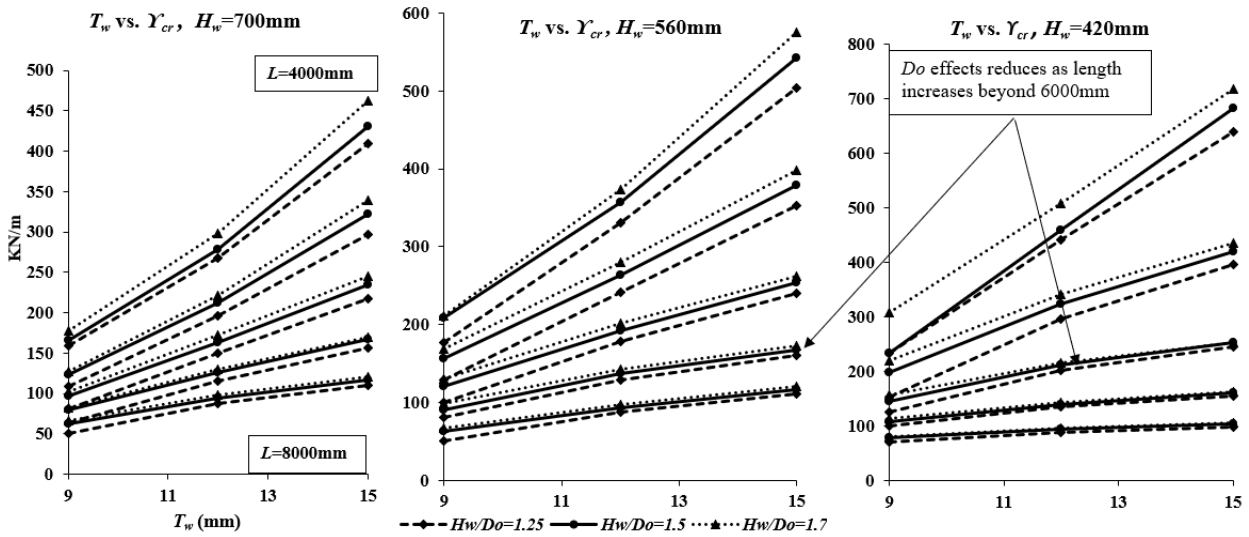

Figure 9: Effects of increasing the F_w from 162mm to 270mm from Figure 7

Figure 10 compared the effects of varying T_f from 15mm to 25mm. The following was concluded:

- $5.5 \geq L/H_w \leq 7.5$, D_o effects are approximately 10.5% and T_w increases the Υ_{cr} by about 93%.
- $7.5 \geq L/H_w \leq 10.5$, D_o effects are approximately 7.0% and T_w increases the Υ_{cr} by about 72%.
- $10.5 \geq L/H_w \leq 13.5$, D_o effects are approximately 5.1% and T_w increases the Υ_{cr} by about 49%.
- $13.5 \geq L/H_w \leq 19$, D_o effects are approximately 4.0% and T_w increases the Υ_{cr} by about 35%.

Comparing Figures 8 and 10 by increasing the T_f for critical members (e.g., $5.5 \geq L/H_w \leq 7.5$) the load increased is in the region of 53% and for slightly more flexible slender members (e.g., $7.5 \geq L/H_w \leq 10.5$) the T_f effects has increases to 62.3%.

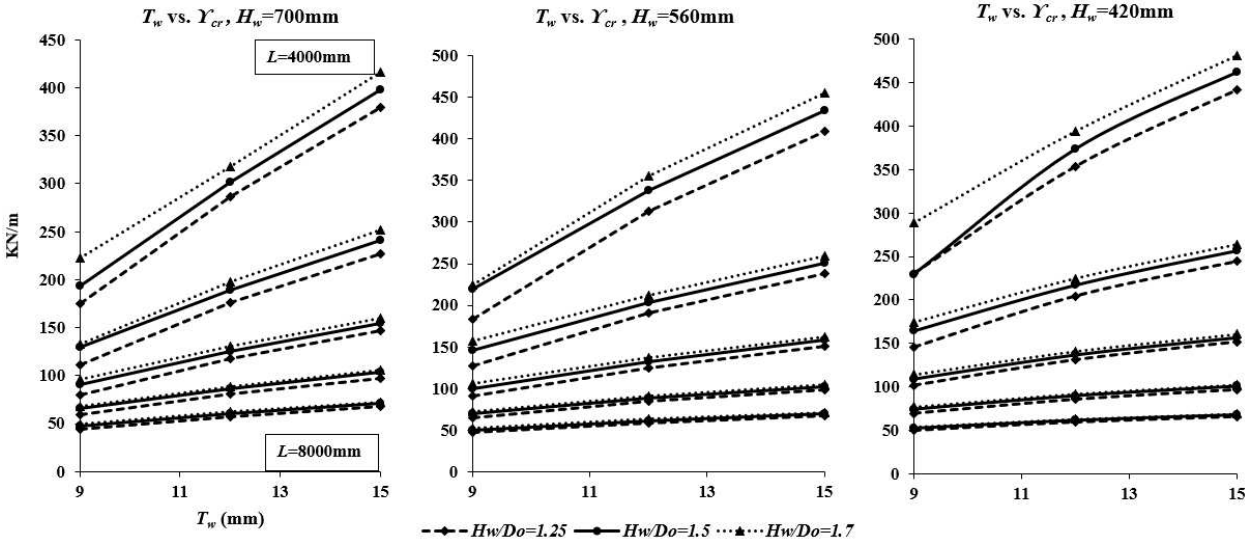

Figure 10: Effects of varying the T_f:15mm to 25mm from Figure 7

Figure 11 considers the effects of the web-post width from $D_o/10$ to $D_o/2.04$. The change in the D_o parameter had little effect on the Υ_{cr} for wider *WP*. The results are outlined as follow:

- $5.5 \geq L/H_w \leq 7.5$, D_o effects are approximately 6% and T_w increases the Υ_{cr} by about 78%.
- $7.5 \geq L/H_w \leq 10.5$, D_o effects are approximately 2.75% and T_w increases the Υ_{cr} by about 37.5%.

Figure 11 shows that for $L/H_w > 10.5$, the other parameters (e.g., *Do, H_w, T_w*) had a minimum effect on the Υ_{cr}. Based on Figures 8 and 11, increasing the $WP = H_w/2.04$ for critical members (e.g., $5.5 \geq L/H_w \leq 7.5$) the load increased is in the region of 20.5% and for slightly more flexible members $7.5 \geq L/H_w \leq 10.5$ the increase is 12.5% from Figure 8.

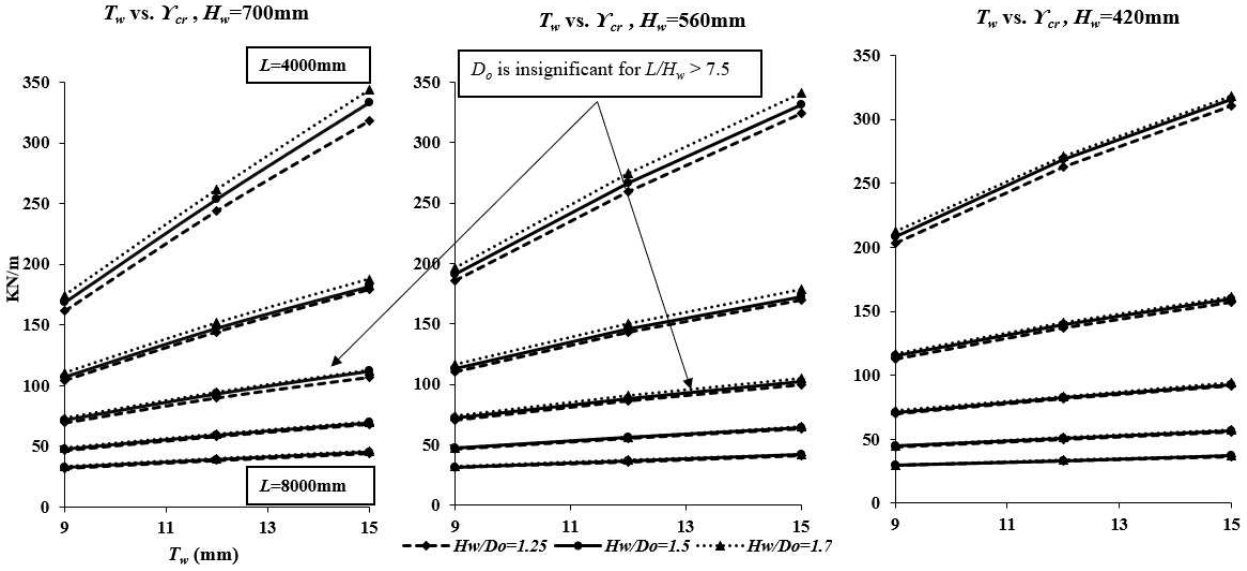

Figure 11: Effects of varying Web-post width: $D_o/10$ to $D_o/2.4$ from Figure 7

4.3 Results of Inelastic Analyses

Inelastic results were analysed similar to Figures 8 to 11, however, the inelastic data were only analysed for L=5m (e.g., L/H_w =7.15 to 12) as it was observed for flexible members (e.g., L/H_w>12) the effects of the other parameters become insignificantly. In addition, the effect of the length is already known from Chung et al. (2003) and Tsavdaridis (2010). The constant variables used for the inelastic analyses are F_y: 355MPa, T_f: 15mm, F_w: 162mm, δ_g: 2.1mm, δ_{LI}: 0.268441mm, D_o/WP:10, ε_y: 0.001775 and ε_f: 0.126175.

In Figure 12, the three graphical responses demonstrate the effects of T_w is the most critical parameter as it controls the web behaviour even when the opening diameter varies. The change in T_w from 9mm to 15mm impacted the inelastic collapse load (P_{CL}) as L/H_w: 7.15, the load increased by 71.9%, L/H_w: 8.9 (60%) and L/H_w: 11.9 (56.5%). The average increase per 1mm change in T_w is approximately 10.5% in P_{CL}. The effects of D_o (e.g., H_w/Do: 1.25 to 1.7) are in the region of 20% which is fairly significant when compared to Figure 8.

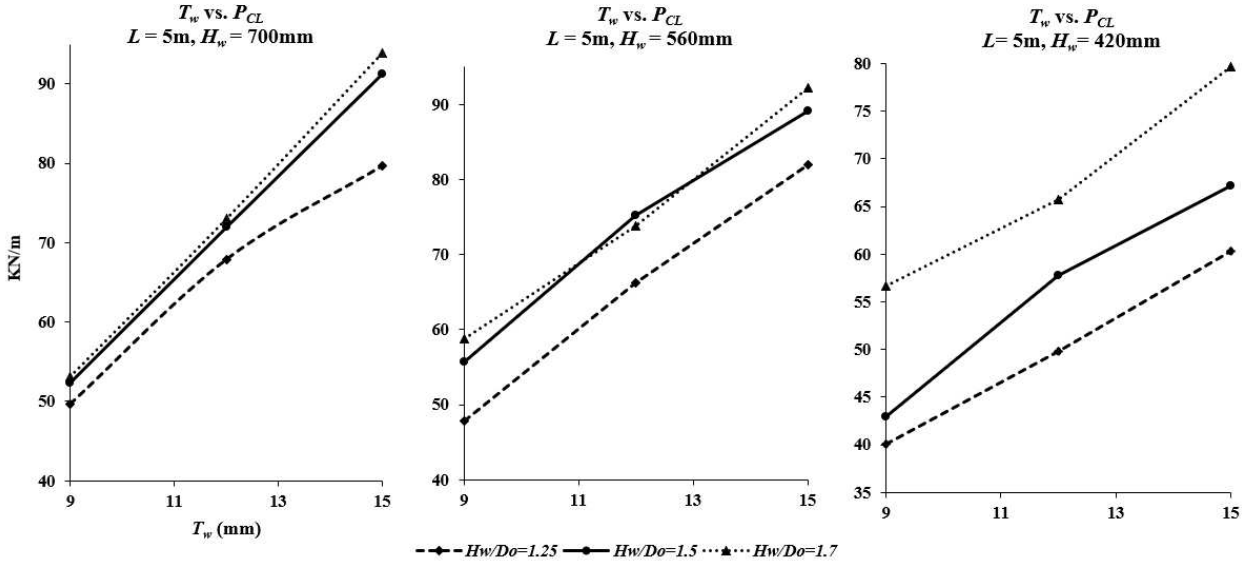

Figure 12: Effects of the H_w on the inelastic load (P_{CL}) with respect to varying T_w

Figure 13 utilised the parameters as Figure 12 however, in this case, the F_w was increased from 162mm to 270mm. The change in the F_w significantly increase the load capacity since first buckling mode experienced a lateral buckling movement of the compression flange therefore with a wider F_w, the δ_g scale in Figure 4 has a lesser impact on the P_{CL}. As such, the effects of T_w for L/H_w = 7.15, load increased by 87.1%, L/H_w = 8.9 (76.1%) and L/H_w = 11.9 (51.5%). The average increase per 1.0 mm change in T_w is approximately 12% in P_{CL} which is similar to Figure 12. The effects of D_o (e.g., H_w/D_o: 1.25 to 1.7) is in the region of 31.9% as such the effects of the D_o increase with the changing in F_w.

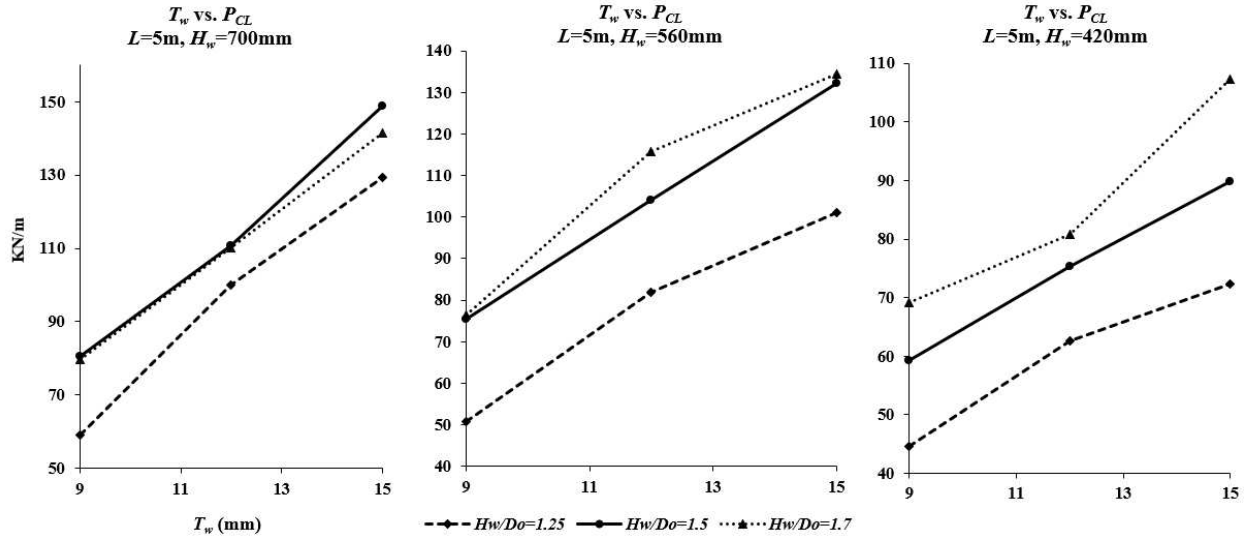

Figure 13: Effects of the F_w: increased from 162mm (as in Figure 12) to 270mm

Figure 14 considered the effects of T_f from 15mm to 25mm. The effects seem to have a similar response to increasing the F_w (e.g., 162mm to 270mm). The change in T_w for L/H_w = 7.15, increased P_{CL} by 79.5%, L/H_w = 8.9 (by 74.2%) and L/H_w = 11.9 (by 52.5%). The average increase per 1.0 mm change in T_w is

approximately 12% in P_{CL} which is similar to Figures 11 and 12. The effects of D_o (e.g., H_w/Do: 1.25 to 1.7) is in the region of 33.6% (similar to Figure 12).

The first graph in Figure 14 (H_w=700mm) shows a strange response when H_w/D_o=1.7. This is because the end distance (L_{Ed}) was only 29mm. The L_{Ed} could not be analysed by these basic graphs as each beam had a different end distance resulted from the aforementioned design limitations.

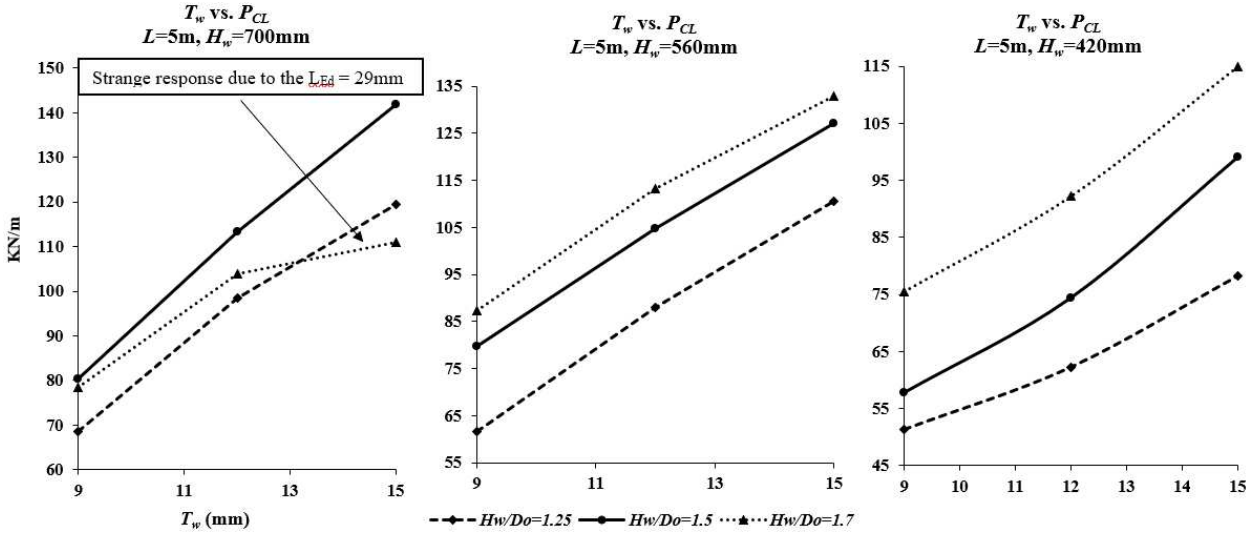

Figure 14: Effects of the T_f: increased from15mm (as in Figure 12) to 25mm

Figure 15 highlights the effects of the narrow L_{Ed}, which influence the load-carrying capacity as stresses are concentrated in the end region very early in the inelastic analysis.

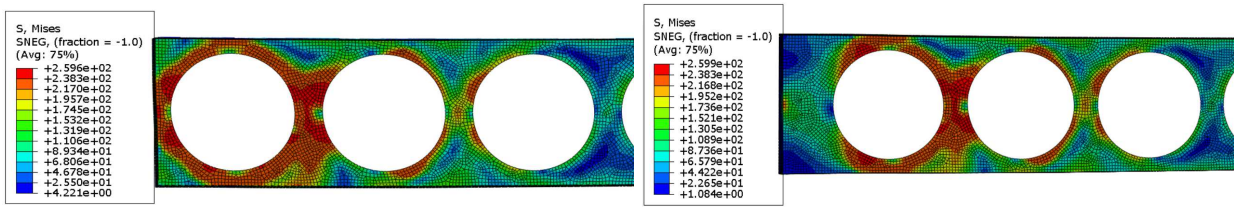

Beam 1 Beam 2

Figure 15: Comparison of stress concentration at maximum LPF for identical beams having varying end-distance (L_{Ed}) of 150mm at maximum LPF. (Collapse load: Beam 1 = 0.37MPa and Beam 2 = 0.40MPa)

Figure 16 highlights the von-mises stresses concentration for varying the wed-post width (e.g., from $D_o/10$ to $D_o/2.04$) for a similar span and section height. The end distance (L_{Ed}) does not influence the load carrying capacity in this comparison.

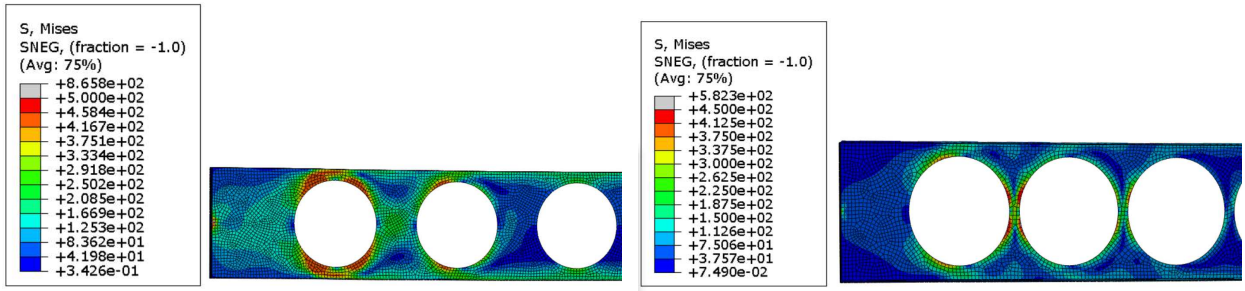

Figure 16: Comparison of stress concentration at maximum LPF for similar beams with varying web-post width. (e.g., $D_o/10$ to $D_o/2.04$)

Figure 17 depicts the effects of the *WP* (e.g., $D_o/10$ to $Do/2.04$). The change in T_w for L/H_w = 7.15, load increased by 77.3%, L/H_w = 8.9 (49.3%) and L/H_w = 11.9 (33.2%). The effects of increasing the *WP* to $D_o/2.04$ resulted in a P_{CL} increase of approximately 17.5% when compared to Figure 12.

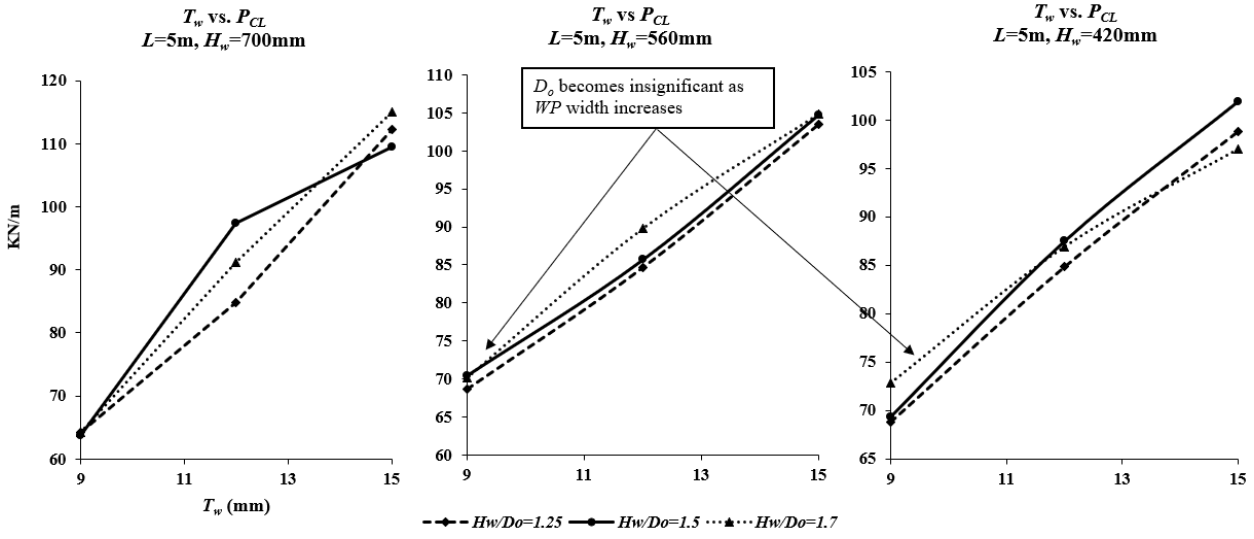

Figure 17: Effects of the Web-post width from $D_o/10$ (as in Figure 12) to $D_o/2$

Figure 18 displays the effects of varying steel strength class from *S235* to *S440* and the variation results in a significant effect on sections that utilised a larger D_o as the effects were in the region of 17%. However, for a mid-range opening diameter (H_w/D_o=1.5), the effect was approximately 5%. The first graph in Figure 18 (*S235* and H_w/D_o=1.7), demonstrates that the beam collapses at a lower load although the D_o is smaller compared to the other plots. This particular beam experienced WP buckling (*WP*=41mm, refer to Table 2) and stresses at the end *WP* (L_{Ed} = 29mm) very early in the analysis.

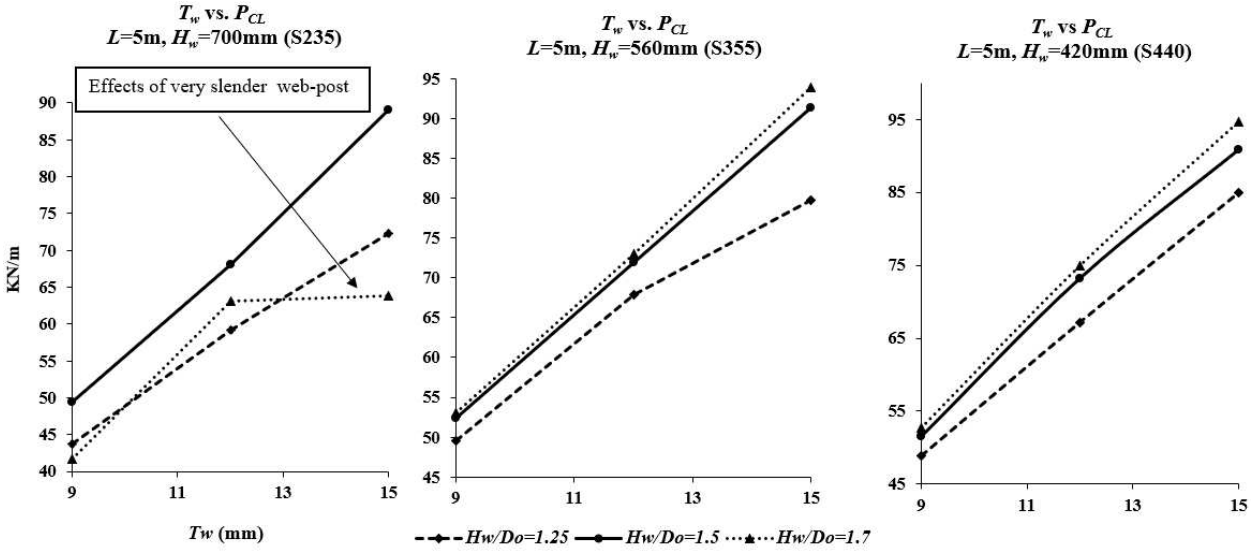

Figure 18: Effects on the steel strength class from *S235* (as in Figure 12) to *S440*

Figure 19 represents the effects of the initial geometrical imperfection. The graphs depict the localised and global imperfection response on the P_{CL} with varying T_w. The effects of the initial imperfection in most cases were less than 5%. Localised web imperfections, however, seemed to have a slightly higher impact on the beam response than the global imperfections.

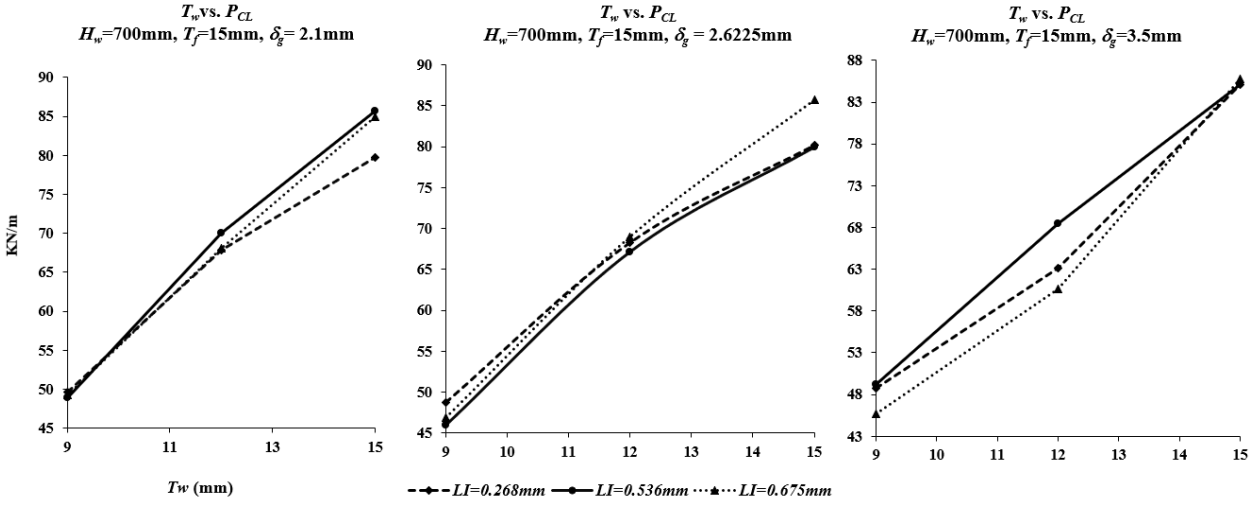

Figure 19: Effects of the variation of the geometrical imperfection *(δ_g* and δ_{LI})

5. Global Stepwise Regression (GSR)

Global stepwise regression (GSR) analysis has the potential of producing statistical models to develop a relationship from a dataset of independent variables to dependent output variables. The process of GSR is iterative by selecting the best independent variables to represent the regression model (Campbell, 2013). Therefore, the combination of independent variables that best correlate to the dependent output variable is identified sequentially by simplifying either adding, deleting or depending on the method to identify which variable has the greatest impact.

Figure 20 highlights the global impact of each parameter on the Υ_{cr} and P_{CL}. In Figure 20a, the influences are L: 57.32%, F_w: 18.1%, T_w: 14.25%, T_f: 5.64%, D_o: 2.58% and L_{Ed}:0.06%. In Figure 20b, the influences are L: 35.92%, T_w: 18.29%, F_w: 15.86%, WP: 14.93%, T_f: 5.96%, D_o: 4.98%, H_w: 2.59% and L_{Ed}: 1.47%.

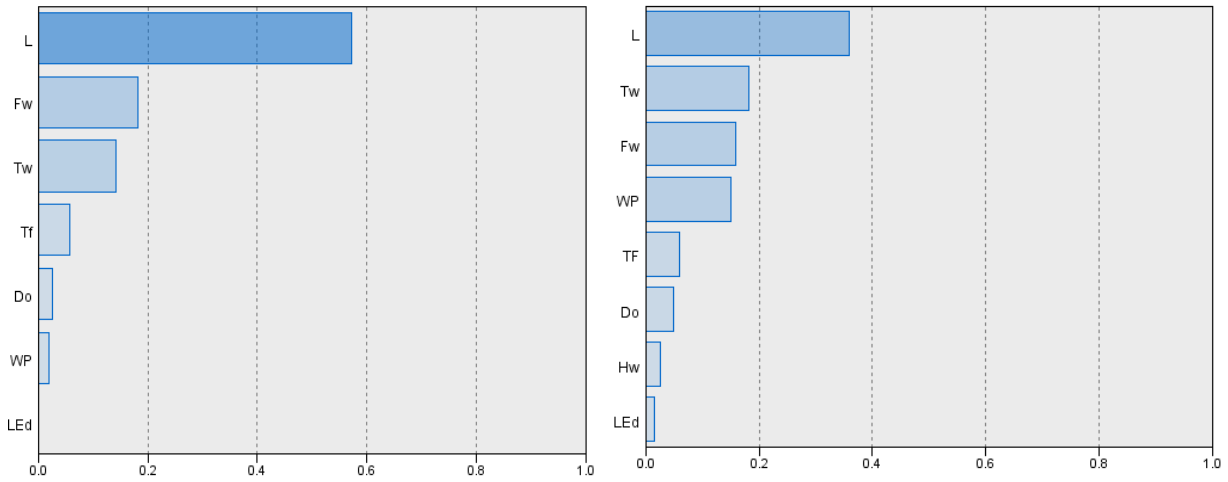

(a.) (b.)

Figure 20: Important independent parameters impact on (a) Υ_{cr} and (b) P_{CL}

Figure 21 considers a fixed length of beam to study the influences of each individual parameters globally. The effects of the parameters in Figure 21a for Υ_{cr} shows that F_w: 42.38%, T_w: 33.37, T_f: 13.21, D_o: 5.98%, WP: 4.86% and L_{Ed}: 0.19%. Similarly, in Figure 21.b shows the effects of P_{CL} are F_w: 28.18%, T_w: 28.01%, WP: 24.71%, T_f: 10.5%, D_o: 6.1%, H_w:1.92%, L_{Ed}: 0.54% and δ_l:0.04%.

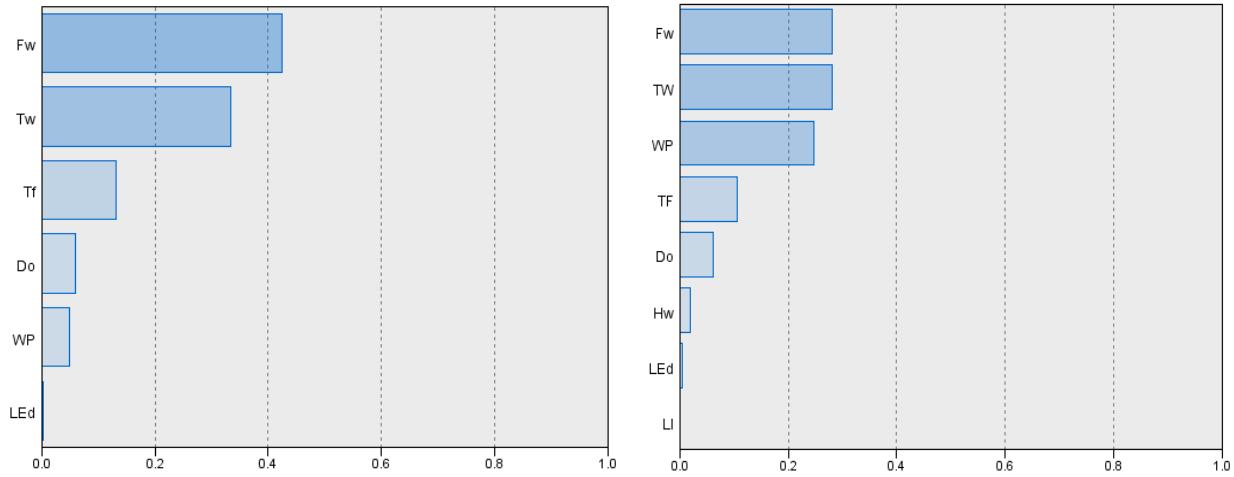

(a.) (b.)

Figure 21: Important independent parameters impact on (a) Υ_{cr} and (b) P_{CL}

6. Discussion

To summarise, when D_o changes from $H_w/1.25$ to $H_w/1.7$ the Υ_{cr} increased by approximately 10.5% for critical members ($5.5 \geq L/H_w \leq 7.5$). Similarly, increasing the WP width from $D_o/10$ to $D_o/2.04$ resulted in an increase in the Υ_{cr} by approximately 20.5% and the effect of the D_o becomes trivial. In collapse analysis, when D_o changes from $H_w/1.25$ to $H_w/1.7$ resulted in an increase in the P_{CL} by approximately 20%. Also, changing the web-post width from $D_o/10$ to $D_o/2.04$ resulted in an increase in the P_{CL} by approximately 17.5% for slender sections (e.g., $L/H_w = 7.15$ *to* 9.0). The influence of the load-carrying capacity due to the initial conditions was observed to be lower than 5% for any geometrical imperfection. The influence of the steel yield strength (from *S235* to *S440*) was approximately 17% but only for the larger diameter

($D_o=H_w/1.25$) of web openings or when $WP=D_o/10$. For any other cases, the influence of the steel yield strength was insignificant.

In addition, the GSR study demonstrated that Υ_{cr} is insensitive (≈ 5%) to a varying perforation geometry but sensitive to the flange (F_w and T_f) and T_w geometry. However, for the collapse analysis, WP influences the P_{CL} greatly at 24.7%. This analysis concludes that the consideration of alternative web opening shapes is possible, without compromising the capacity of the steel perforated beams and similar performances are anticipated overall. Consequently, the work of various researchers on perforated beams with non-standard web opening configurations should be considered for the Eurocode 3 compliance without the need for drastic updates. Similarly, the coherent mass data results generated in this paper can be used to derive sophisticated closed-form solutions. For example, the data has been already used to develop an artificial neural network-based formula (Abambres et al., 2018).

7. Conclusions

From this comprehensive FE investigation, it was concluded that the most critical parameter for both global elastic and inelastic analyses of cellular beams is the web thickness. Since the beams were not laterally restraint, the first buckling mode is a result of the lateral movement of the compression flange, and consequently, both the T_f and F_w had significant impact on the beam response.

A comparison study was also established between the SCI P355 analytical method and the mass FE data, which demonstrated the level of conservatism of the former. It is also noticeable that the elastic and inelastic FE results are not fluctuating together, with the inelastic analyses comparing very well with the SCI P355 calculation which suggests that cellular beams are vastly behaving inelastically, thus design approaches using elastic design should be abandoned.

Notation

The following symbols are used in this paper:

D_o: Perforation diameter
E: Modulus of Elasticity
E_t: Tangential Modulus
ε_y: Initial strain of steel
ε_f: Final yield strain of steel
f_u: Ultimate Stress
f_y: Yield stress of steel
F_w: Width of flange
δ_G: Global geometric imperfection
H: Total depth of the member
H_w: Height of web (centre of web to web)
L: Length of beams
L_{Ed}: End web-post distance (end perforation to support)
δ_{LI}: Local geometric imperfection
$M_R=M_L$: local moment at the perforation
M_h: Local moment at the web-post
σ_R: Residual stresses

P_{CL}: Inelastic collaspe load
S_o: Center to center of openings.
T_f: Flange thickness
T_w: Web thickness
γ: Material proof stresses of 0.1% and 0.2% in imperfection
Υ_{cr}: elastic bucle load (N/mm)
$V_L = V_R$: Local shear force at the perforation
$V_t = V_b$: Local shear force at the top and botoom tee-section.
V_h: Local hpzontal shear force at the web-post
WP: Width of Web post
UX, UZ, UY: movement in different plane in model space (Figure 3) *UZ*: perpendicular to web, *UX*: along beam and *UY*: perendicular to flange.
ΔF_{load}*:* incremental load

Data Availability

Both datasets are available at https://osf.io/5jxut/

For Python scripting contact with corresponding author of the paper at k.tsavdaridis@leeds.ac.uk

References

Abambres M, Rajana K, Tsavdaridis KD and Ribeiro T (2018) Neural Network-Based Formula for the Buckling Load Prediction of I-Section Cellular Steel Beams. *Computers*. 8(1), 2.

Altfillisch MD, Cooke BR, and Toprac AA (1957) An Investigation of open web expanded beams, *Welding Research*, 22(2).

Akrami V and Erfani S (2016) Review and assessment of design methodologies for perforated steel beams, *Journal of Structural Engineering*, 142(2), 1-14.

American Institute of Steel Construction (2010) Specification for Structural Steel Buildings (ANSI/AISC 360-10), American Institute of Steel Construction, Chicago.

Bower JE (1968) Design of beams with web openings, *Journal of the Structural Division*, Proceedings of the American Society of Civil Engineers, 94(3), 783-808.

Bradford MA (1992) Lateral-distortional buckling of steel I-section members, *Journal of Constructional Steel Research*, 23(1-3), 97-116.

Bradford MA (1998) Distortional buckling of elastically restrained cantilevers, *Journal of Constructional Steel Research*, 47(1-2), 3-18.

Campbell M (2013) Statistics at Square Two. New York, NY: John Wiley & Sons.

London: GBR: BMJ Publishing Group.

Chung K F, Liu TCH and Ko ACH (2001) Investigation on Vierendeel mechanism in steel beams with circular web openings. *Journal of Constructional Steel Research,* 57, 467-490.

Chung KF, Liu CH and Ko ACH (2003) Steel beams with large web openings of various shapes and sizes: an empirical design method using a generalized moment-shear interaction curve, *Journal of Construction Steel Research*, 59(9), 1177-1200.

Clawson WC and Darwin D (1980) Composite beams with web openings, Kansas State University, Kansas.

Darwin D (1990). Steel and composite beams with web opening, *Steel Design Guide Series 2*, AISC, Chicago.

Dassault Systèmes (2011) ABAQUS 6.11, Abaqus/CAE user's manual, Dassault Systems, USA.

Dassault Systèmes Simulia Corp (2017). ABAQUS CAE (2017). [Software].

Dawson RG and Walker AC (1972). Post-buckling of geometrically imperfect plates, *Journal of Structural Engineering*, 98(1), 75-94.

Ellobody E (2011) Interaction of buckling modes in castellated steel beams, *Journal of Constructional Steel Research*, 67(2011), 814-825.

Ellobody E (2012) Nonlinear analysis of cellular steel beams under combined buckling modes, *Thin-Walled Structures*, 52, 66-79.

Ellobody E (2017). Interaction of buckling modes in railway plate girder steel bridges, *Thin-Walled Structures*, 115, 58-75.

Gardner L and Nethercot DA (2004) Numerical modelling of stainless-steel structural components- A consistent approach, *Journal of Structural Engineering*, 130(10), 1586-1601.

Hesham Martini MIM (2011) Elasto-plastic lateral torsional buckling of steel beams with perforated web, Ph.D. Thesis, United Arab Emirates University.

Hosain MU and Speirs WG (1971) Failure of castellated beams due to rupture of welded joints, Acier-Stahl-Steel, 36(1), 34-40.

Kerdal D and Nethercot DA (1984) Failure modes for castellated beams, *Journal of Constructional Steel Research*, 4(1984), 295-315.

Kingman JJ, Tsavdaridis KD and Toropov VV (2015) Applications of Topology Optimisation in Structural Engineering: High-rise Buildings & Steel Components, *Jordan Journal of Civil Engineering*, 9(3), 335-357.

Kolosowski J (1964) Stresses and deflections in castellated beams, *The Structural Engineer*, 42 (1).

Kwani S and Wijaya PK (2017). Lateral torsional buckling of castellated beams analysed using the collapse analysis, *Procedia Engineering*, 171(2017), 813-820.

Lawson RM (1987) Design for openings in the webs of composite beams SCI P068. Steel Construction Institute, Berkshire, UK.

Lawson RM and Hicks SJ (2011) Design of composite beams with large openings SCI P355. Steel Construction Institute, Berkshire, UK.

Lucas WK and Darwin D (1990) Steel and composite beams with web openings. The American Iron and Steel Institute, Kansas.

Maraveas C, Tsavdaridis KD and Nadjai A (2017) Fire Resistance of Partially Unprotected Ultra Shallow Floor Beams (USFB): A Numerical Investigation, *Fire Technology*, 53(2), 609-627.

Redwood RG and McCuthcheon JO (1968) Beam tests with unreinforced web openings, *Journal of the Structural Division*, 94, 1-17.

Redwood RG, Baranda H and Daly MJ (1978) Tests of thin-webbed beams with unreinforced holes, *Journal of the Structural Division*, 104(3), 577-595.

Sweedan A (2011) Elastic lateral stability of I-shaped cellular steel beams. Journal of Constructional Steel Research, 67(2), 151-163.

575 SEI/ASCE (1998) Specifications for structural steel beams with openings, SEI/ASCE 23-97, ASCE, Reston
576 VA.
577 Sonck D (2014). Global buckling of castellated and cellular steel beams and columns, Ph.D. Thesis, Ghent
578 University.
579 Surtees JO and Lui Z (1995) Report of loading tests on cellform beams. Research Report, University of
580 Leeds, Leeds.
581 Taras A (2010) Contribution to the Development of Consistent Stability Design Rules for Steel Members.
582 Phd thesis, Graz University of Technology
583 Toprac AA and Cooke BR (1959) An experimental investigation of open-web beams, Welding Research
584 Council, New York.
585 Tsavdaridis KD (2010) Structural performance of perforated steel beams with novel web openings and with
586 partial concrete encasement, Ph.D. Thesis, City University London.
587 Tsavdaridis KD and D'Mello C (2009) Finite Element Investigation of Perforated Beams with Different
588 Web Opening Configurations. The 6th International Conference on Advances is Steel Structures (ICASS
589 2009). 16-18 December 2009, Hong Kong, China, 213-220.
590 Tsavdaridis KD and D'Mello C (2011) Web buckling study of the behaviour and strength of perforated steel
591 beams with different novel web opening shapes. *Journal of Constructional Steel Research*, 67 (10), 1605-
592 20.
593 Tsavdaridis KD and D'Mello C (2012) Vierendeel bending study of perforated steel beams with various
594 novel web opening shapes through non-linear finite element analyses. *Journal of Structural Engineering*,
595 138 (10), 1214- 30.
596 Tsavdaridis KD, D'Mello C and Huo BY (2013) Experimental and Computational Study of Vertical Shear
597 Behaviour of Partially Encased Perforated Steel Beams. *Engineering Structures*. 56, 805-822.
598 Tsavdaridis KD and Galiatsatos G (2015) Assessment of Cellular Beams with Transverse Stiffeners and
599 Closely Spaced Web Openings. *Thin-Walled Structures*. 94, 636-650.
600 Verweij JG (2010) Cellular beam-columns in portal frame structures. MSc. Thesis, Delft University of
601 Technology, Holland.
602 Huo BY, D'Mello C and Tsavdaridis KD (2010) Experimental and Analytical Study of Push-out Shear
603 Tests in Ultra Shallow Floor Beams. The 34th International Association for Bridge and Structural
604 Engineering Symposium (IABSE 2010). 22-24 September 2010, Venice, Italy, IABSE Proceedings, 31-38.
605 Ward JK (1990) Design of composite and non-composite cellular beams SCI P100. Steel Construction
606 Institute, Berkshire, UK.
607 Zirakian T and Showkati H (2006) Distortional buckling of castellated beams, *Journal of Constructional*
608 *Steel Research*, 62(9), 863-871.
609 Zirakian T (2008) Elastic distortional buckling of doubly symmetric I-shaped flexural members with
610 slender webs, *Thin-Walled Structures*, 46(5), 466-475.